

Neuroevolution Surpasses Stochastic Gradient Descent for Physics-Informed Neural Networks

Nicholas Sung Wei Yong
Centre for Frontier AI Research
(CFAR)

Agency for Science, Technology and
Research (A*STAR)
1 Fusionopolis Way, #16-16 Connexis,
Singapore 138632, Republic of
Singapore
nsung001@e.ntu.edu.sg

Jian Cheng Wong
Institute of High Performance
Computing (IHPC)

Agency for Science, Technology and
Research (A*STAR)
1 Fusionopolis Way, #16-16 Connexis,
Singapore 138632, Republic of
Singapore
wongj@ihpc.a-star.edu.sg

Pao-Hsiung Chiu
Institute of High Performance
Computing (IHPC)

Agency for Science, Technology and
Research (A*STAR)
1 Fusionopolis Way, #16-16 Connexis,
Singapore 138632, Republic of
Singapore
chiuph@ihpc.a-star.edu.sg

Abhishek Gupta
Singapore Institute of Manufacturing
Technology (SIMTech)
Agency for Science, Technology and
Research (A*STAR)
1 Fusionopolis Way, #16-16 Connexis,
Singapore 138632, Republic of
Singapore
abhishek_gupta@simtech.a-star.edu.sg

Chin Chun Ooi
Institute of High Performance
Computing (IHPC)
Agency for Science, Technology and
Research (A*STAR)
1 Fusionopolis Way, #16-16 Connexis,
Singapore 138632, Republic of
Singapore
ooicc@cfar.a-star.edu.sg

Yew-Soon Ong
School of Computer Science and
Engineering (SCSE)
Nanyang Technological University
(NTU)
50 Nanyang Avenue, Singapore
639798, Republic of Singapore
asysong@ntu.edu.sg

Abstract—The potential of learned models for fundamental scientific research and discovery is drawing increasing attention. Physics-informed neural networks (PINNs), where the loss function directly embeds governing equations of scientific phenomena, is one of the key techniques at the forefront of recent advances. These models are typically trained using stochastic gradient descent, akin to their standard deep learning counterparts. However, in this paper, we carry out a simple analysis showing that the loss functions arising in PINNs lead to a high degree of complexity and ruggedness that may not be conducive for gradient-descent and its variants. It is therefore clear that the use of neuro-evolutionary algorithms as alternatives to gradient descent for PINNs may be a better choice. Our claim is strongly supported herein by benchmark problems and baseline results demonstrating that convergence rates achieved by neuroevolution can indeed surpass that of gradient descent for PINN training. Furthermore, implementing neuroevolution with JAX leads to orders of magnitude speedup relative to standard implementations.

Keywords— Neuro-evolutionary algorithms, stochastic gradient descent, physics-informed neural networks.

I. INTRODUCTION

A physics-informed neural network (PINN) is a type of deep learning model that incorporates physical laws and constraints into the training process. PINNs combine the expressive power of neural networks with the guarantees accorded by compliance with physical laws and principles to ensure that the predictions of the network remain consistent with known physical laws and constraints [1]. This allows PINNs to generalize better and make accurate predictions even on test-time data. The utility of this framework has been demonstrated on various complex scientific and engineering problems, towards purposes such as predicting the behaviour of physical systems, modelling the properties of materials, and assimilating data from experiments and simulations [2].

While promising and very effective when successfully learned, PINN training has been shown to be complex, and prone to various failure mechanisms even when state-of-the-art stochastic gradient descent-based (SGD-based) methods are used for training [3]. A variety of challenges have been identified in previous work, especially when local optimization methods like gradient descent algorithms are used. These include the need for proper balancing of the competing loss terms present in a PINN’s objective function [4], the impact of learning biases [5], and sensitivity to initialization [6] and a consequent inability to escape spurious local minima [7–9].

This paper aims to gain further insights as to the spurious local minima traps by visualizing the PINN loss landscape at model initialization. Based on the observed characteristics of the function landscape, we make a strong case for the evaluation of *evolutionary algorithms* for PINN training in place of local methods like stochastic gradient descent. Importantly, evolutionary algorithms are a subset of artificial intelligence methods that are commonly used to approximate solutions to nonconvex optimization problems with multiple local optima. By using a population-based approach and applying evolutionary principles, they can explore the space of possible solutions effectively [10]. This can be especially useful when dealing with complex or nonlinear systems. When applied to neural nets, the process of such evolutionary algorithms is referred to as *neuroevolution*. In the context of PINNs, neuroevolution can be used to find a near optimal configuration of the network’s parameters in order to more accurately model a given physical system [11], and may present certain advantages over conventional gradient descent methodologies in view of their complicated optimization landscapes [12]. However, despite the potential benefits of using neuroevolution for training PINNs, there has been relatively little research in this area, and this work is among the first to embark on a systematic evaluation of the effectiveness of neuroevolution relative to the more commonly used SGD.

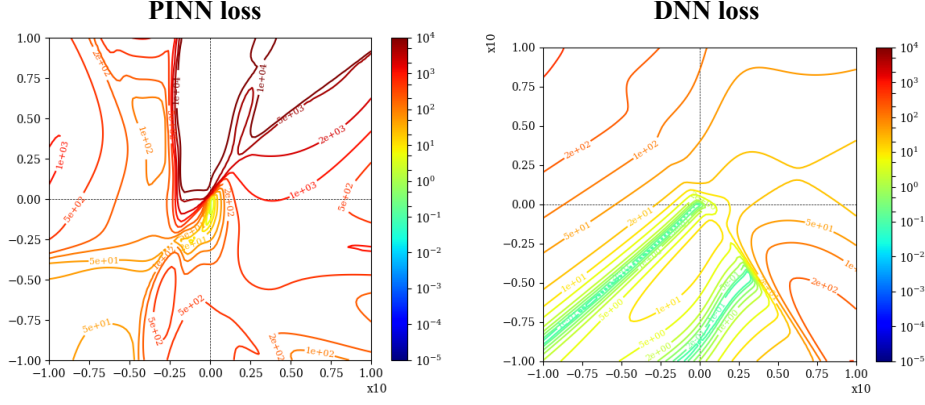


Fig. 1. The plots contrast the local loss landscapes of the PINN and the DNN after 100,000 training iterations on the convection-diffusion differential equation $6u_x = u_{xx}$. The losses are plotted along the first two principal Hessian directions.

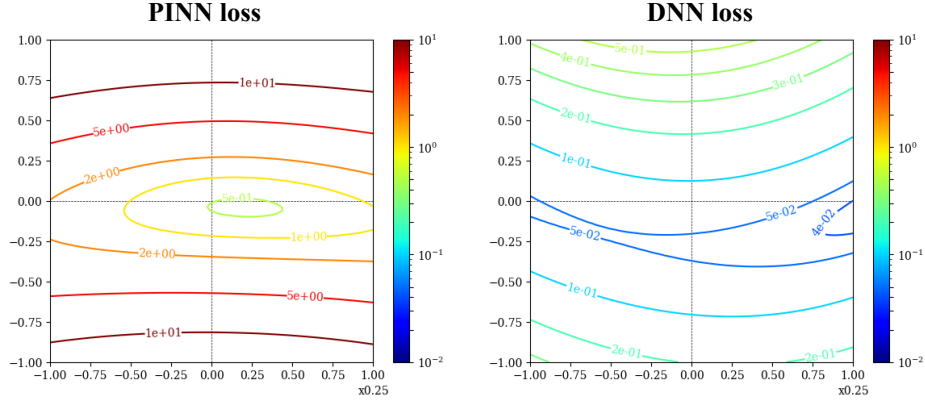


Fig. 2. A zoomed-in view of the local loss landscapes of the PINN and the DNN at Xavier model initialization, plotted along the first two principal Hessian directions.

To this end, we present a set of five benchmark problems, and systematically evaluate the performance and speed of evolutionary algorithms, specifically the widely adopted Covariance Matrix Adaptation Evolution Strategy (CMA-ES) [13], against SGD. The loss and training time of CMA-ES run on JAX [14], CMA-ES run on TensorFlow (with and without GPU acceleration) [15], and SGD run on JAX are reported for the five benchmark problems. By comparing the results of these implementations, we then objectively assess the relative effectiveness and efficiency when using either evolutionary algorithms or stochastic gradient descent for training PINNs. Notably, neuroevolution consistently provides competitive or superior convergence performance, with JAX supporting orders of magnitude speedup relative to standard implementations. These benchmarks and baseline results are therefore expected to motivate the development and testing of further state-of-the-art neuroevolutionary algorithms in the future, especially those crafted for application to PINNs.

The remainder of the paper is organized as follows. Section 2 presents a simple landscape study of the PINN loss, outlining the potential and capacity of neuroevolution to address the challenges faced by gradient-based learning. Section 3 describes the optimization algorithms and deep learning frameworks used. Sections 4 and 5 introduce the benchmark problems and performance metrics, respectively. Section 6 evaluates the performance and speed of CMA-ES against SGD in solving the five benchmark problems. Finally, Section 7 presents concluding remarks and direction for future research.

II. EMERGING POTENTIAL OF NEUROEVOLUTION FOR PINNS

In this section, we first present the problem setup for PINNs, contrasting it to standard deep neural networks (DNNs). The loss landscapes of the two models are then analyzed, making the case for neuroevolution as a strong candidate in the unique context of PINN training.

2.1 PINN vs DNN loss functions

A typical PINN uses a multilayer perceptron (MLP) representation, $\hat{u}(x, t; \mathbf{w})$ to model the dynamic scalar quantity of a physical system (u) in space ($x \in \Omega$) and time ($t \in [0, T]$). The network parameters (\mathbf{w}) are optimized for this purpose. Additionally, u must adhere to known mathematical constraints, such as partial differential equations (PDEs) of the general form:

$$\mathcal{N}_t[u(x, t)] + \mathcal{N}_x[u(x, t)] = 0, \quad x \in \Omega, t \in [0, T], \quad (1)$$

$$u(x, 0) = u_0(x), \quad x \in \Omega, \quad (2)$$

$$\mathcal{B}[u(x, t)] = g(x, t), \quad x \in \partial\Omega, t \in [0, T], \quad (3)$$

Here, the temporal derivative is represented by $\mathcal{N}_t[\cdot]$ and the general nonlinear differential operator $\mathcal{N}_x[\cdot]$ can include any combination of nonlinear terms of spatial derivatives. The initial state of the system at time $t=0$ is given by $u_0(x)$, and the boundary operator $\mathcal{B}[\cdot]$ ensures that the desired boundary condition $g(x, t)$ is met at the domain boundary ($\partial\Omega$). $\mathcal{B}[\cdot]$ can either be an identity operator or a differential operator.

The loss function of a PINN is then defined as:

$$\mathcal{L}_{PINN} = \mathcal{L}_{PDE} + \mathcal{L}_{IC} + \mathcal{L}_{BC} \quad (4)$$

$$\mathcal{L}_{PDE} = \|\hat{u}_t(\cdot; \mathbf{w}) + \mathcal{N}_x[\hat{u}(\cdot; \mathbf{w})]\|_{\Omega \times [0, T]}^2 \quad (5)$$

$$\mathcal{L}_{IC} = \|\hat{u}(\cdot, 0; \mathbf{w}) - u_0\|_{\Omega}^2 \quad (6)$$

$$\mathcal{L}_{BC} = \|\mathcal{B}[\hat{u}(\cdot; \mathbf{w})] - g(\cdot)\|_{\partial\Omega \times [0, T]}^2 \quad (7)$$

The PINN loss (4) sums the PDE residuals (5) across the input domain $\Omega \times [0, T]$, the mean squared error at the initial condition (6) and boundary condition at the domain boundary (7). Although the PINN loss (\mathcal{L}_{PINN}) is formulated over the entire continuous domain, for practical purposes, the residuals are determined at a finite set of n collocation points $D = \{(x_i, t_i)\}_{i=1}^n$.

In contrast to PINNs where there is no need for additional labelled training data in the domain of interest, the loss function of a standard DNN is defined as:

$$\mathcal{L}_{DNN} = \frac{1}{n} \sum_{i=1}^n (u_i - \hat{u}_i)^2 \quad (8)$$

The DNN loss (8) computes the well-known mean squared error between the DNN output \hat{u} against the target u over n labelled collocation points.

2.2 Complexity of PINN Loss Landscapes

We trained both the DNN and PINN for an instantiation of the one-dimensional convection-diffusion equation defined as $6u_x = u_{xx}$. In both cases, the networks were trained with the same optimizer, collocation points, boundary points and network architecture. We then projected the training loss values in the plane spanned by the first two principal Hessian directions [16] as illustrated in Fig. 1.

After 100,000 training iterations, we observe a much higher degree of complexity and ruggedness of the loss landscape for PINN compared to DNN. These loss landscapes provide early evidence that the loss function in PINN is indeed more complex in comparison to DNN, thereby raising questions about the suitability of conventional gradient-based learning algorithms in this area of application.

2.3 Analysing the Loss Landscapes at Model Initialization

In addition to the rugged and complex loss landscape that a PINN has to encounter during training, Wong et al. [6] have shown in earlier work that PINNs are susceptible to being trapped in a deceptive local minima even at the point of model initialization. The following proposition from [6] highlights this point.

Proposition 1. Let $\hat{u}(x; \mathbf{w})$ be a PINN with L fully connected layers, N neurons per layer, activation function $f=\tanh$, and parameters \mathbf{w} . Let all the dense layers be initialized by the Xavier method for network weights, i.e., w_l 's are i.i.d. $\mathcal{N}(0, \frac{2}{fan_{in} + fan_{out}})$, where fan_{in} and fan_{out} are the number of inputs and outputs for the dense layer. Then, as $N \rightarrow \infty$, $\hat{u}(x; \mathbf{w})$ trivially satisfies arbitrary differential equations of the form $F(\frac{\partial u}{\partial x}, \frac{\partial^2 u}{\partial x^2}, \dots, \frac{\partial^k u}{\partial x^k}) = 0$ where $F(\varphi_1, \varphi_2, \varphi_3, \dots) = \sum_i a_i \varphi_i + \sum_{i \leq j} b_{ij} \varphi_i \varphi_j + \sum_{i \leq j \leq k} c_{ijk} \varphi_i \varphi_j \varphi_k + \dots$, with probability 1 at initialization.

The above proposition was proven in the limit of infinitely wide layers. It says that a PINN tends to prematurely satisfy certain (commonly occurring) PDEs at initialization without accounting for boundary conditions, thus hinting at a deceptive local minimum of the overall PINN loss (4) with zero PDE loss (5) but violations in (6) or (7). In this paper, we empirically investigate and corroborate the validity of this observation in the context of finite-width PINNs.

Using the same problem set-up as in Section 2.2, the loss landscapes of the PINN and DNN at the same initialization point are visualized in Fig. 2 along the first two principal Hessian directions, and the first two principal eigenvalues along those directions were obtained. The first two principal eigenvalues for PINN were found to be 509.6 and 35.7, while those for DNN were 9.9 and -1.5. The two large positive eigenvalues for PINN indicate that the PINN at initialization is indeed near a local minimum, as is consistent with Proposition 1. In contrast, the presence of a negative eigenvalue for DNN indicates that there are descent paths available for a gradient-based learning algorithm to start moving towards a potential good solution.

Indeed, when we further plot the PINN and DNN predicted outputs after 5,000 training iterations (Fig. 3), we observed that the DNN can already approximate the ground truth reasonably well, whereas the PINN model is clearly still far from the solution, and appears to be trapped in a local minimum. This further provides evidence that the optimization process is trapped in the vicinity of a deceptive local minimum at initialization. The flatness of the PINN output also suggests that this local minimum is one that only minimizes the PDE residual terms, without satisfying the boundary conditions as is required for the true solution, as previously documented by Wong et al. [6].

The lack of a nearby, deleterious local minimum from initialization in the DNN approach makes it suitable for optimization using SGD. However, PINNs have the potential

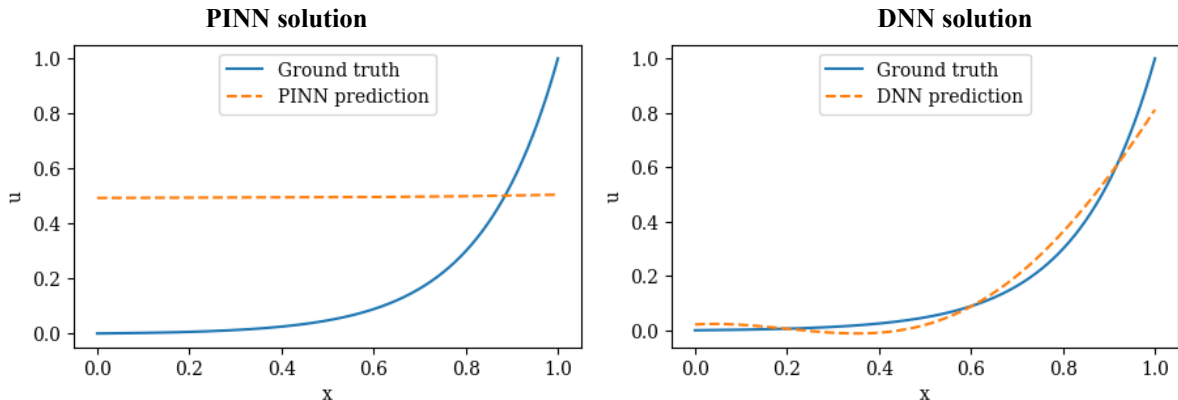


Fig. 3. The solution plot of PINN and the DNN after 5,000 training iterations.

for spurious local minima close by that only satisfy one of the multiple loss terms, posing difficulties for optimization using SGD, which is a local optimization method. To address this challenge, global optimization methods, such as neuroevolution, are investigated due to their greater capability for exploring the loss landscape and escaping such local minima.

III. OPTIMIZATION ALGORITHMS AND DEEP LEARNING FRAMEWORKS

The aim of this study is to compare the performance when using CMA-ES and SGD for solving PINNs. Two commonly used backend implementations (JAX and TensorFlow) are used to build the PINN models, and their relative performances are also compared for the same baseline algorithm (CMA-ES). For the sake of consistency across comparisons, all results are obtained from runs on a workstation with an Intel Xeon W-2275 Processor (19.25M Cache, 3.30 GHz, 14 cores) CPU and two NVIDIA GeForce RTX 3090 GPUs.

Table I summarises the various combinations of PINN optimization algorithms and deep learning framework compared in this work. These combinations have been selected to evaluate i) the acceleration of JAX relative to TensorFlow implementations (with and without GPU acceleration); ii) the performance and training time metrics when using CMA-ES and SGD on the JAX platform (with GPU acceleration) for training PINNs.

Table I: Summary of optimization methods used in current study.

Method	Optimization algorithm		Deep learning framework		GPU-acceleration
	CMA-ES	SGD	JAX	TensorFlow	
1	√			√	
2	√			√	√
3	√		√		√
4		√	√		√

3.1 Optimization Algorithms

In this paper, we use the Covariance Matrix Adaptation Evolution Strategy (CMA-ES) to train PINNs. CMA-ES is a population-based, gradient-free optimization algorithm that can be used to approach the global minimum of any complex objective function defined on a continuous search space. It does not require the calculation of exact gradients or other derivatives of the objective function, and instead uses a probabilistic model-based search strategy to sample and explore the space of possible solutions, gradually converging towards a region where the global minimum is likely to be located [17].

The key feature of CMA-ES is its ability to adapt the search strategy based on the behaviour of the objective function gleaned from the sampled solutions. As an instantiation of an information-geometric optimization procedure, CMA-ES iteratively updates an estimate of the mean and the covariance matrix of a multivariate Gaussian distribution model from which subsequent candidate solutions are to be sampled and evaluated against the objective function. The spread of the solutions allows the algorithm to more effectively explore the space of possible solutions, thereby avoiding the propensity of (point-based) optimization techniques to get stuck in local minima. This adaptive search strategy makes CMA-ES particularly well-suited for complex

optimization problems with multiple local optima, such as those encountered in deep learning with nonconvex loss functions. Its well-established performance across many domains motivates the choice of CMA-ES as a competitive baseline evolutionary algorithm for study in this work. Results from CMA-ES are compared against SGD, which is a hugely popular point-based optimization algorithm used to train deep learning models (especially deep neural networks).

3.2 Deep Learning Framework

Both JAX and TensorFlow are popular libraries for deep learning research and development. They provide tools and APIs for implementing and training deep learning models. Both libraries allow users to flexibly define, train, and run deep learning models, and both can be run on a wide range of hardware platforms, including CPUs, GPUs, and TPUs. However, there are some key differences between the two libraries that make JAX generally faster and more efficient than TensorFlow [18].

One major difference is the way JAX and TensorFlow handle automatic differentiation. JAX uses the autodiff system, Autograd, to automatically compute gradients of functions, while TensorFlow uses a static graph representation and reverse-mode automatic differentiation to compute gradients. This means that JAX is able to differentiate functions that are defined dynamically at runtime, while TensorFlow requires the gradient computation to be specified in advance, as part of the model's computational graph [19].

Another key difference is the implementation of JAX and TensorFlow. JAX uses just-in-time (JIT) compilation to optimize code for specific hardware, allowing it to run operations on CPU, GPU, or TPU without the need to change the code. This makes JAX more flexible and efficient than TensorFlow. Additionally, JAX uses XLA, a domain-specific compiler, to further optimize the performance of deep learning algorithms. This allows JAX to run operations faster than TensorFlow, which uses a more general-purpose compiler [19].

Given these differences, we will validate the performance of JAX and TensorFlow by comparing their relative performances for the same baseline algorithm (CMA-ES).

IV. BENCHMARK PROBLEMS

In this paper, we establish five benchmark problems for PINNs which are representative of real-world phenomena. The detailed definitions of these benchmark problems are summarised in Table II.

These set of benchmark problems were chosen to be diverse in type and application, comprising both ordinary and partial differential equations that describe phenomena in classical mechanics, heat and mass transfer, fluid dynamics and wave propagation (e.g., in acoustics):

Table II: Detailed definitions of benchmark problems.

Problem	Physics / differential equation	Initial condition / boundary condition	Computational domain
1) Convection-diffusion	$vu_x - ku_{xx} = 0$ $v = 6, k = 1$	$u(x = 0) = 0$ $u(x = 1) = 1$	$x \in [0, 1]$
2) Projectile motion	$x_{tt} = 0$ $y_{tt} + g = 0$ $g = 3.7$	(Initial displacement): $x(t = 0) = 0$ $y(t = 0) = 2$ (Initial velocity): $x_t(t = 0) = V_o \cos\left(\frac{\alpha_o \pi}{180}\right)$ $y_t(t = 0) = V_o \sin\left(\frac{\alpha_o \pi}{180}\right)$ $V_o = 10, \alpha_o = 80^\circ$	$t \in [0, 2]$
3) Korteweg-De Vries (KdV)	$u_t + v_1 uu_x + v_2 u_{xxx} = 0$ $v_1 = 1, v_2 = 0.001$	$u(x, t = 0)$ $= \frac{3c_1}{(\cosh(a_1(x - x_1)))^2}$ $+ \frac{3c_2}{(\cosh(a_2(x - x_2)))^2}$ $a_1 = \frac{1}{2} \sqrt{\frac{c_1}{v_2}}, a_2 = \frac{1}{2} \sqrt{\frac{c_2}{v_2}}$ $c_1 = 0.3, c_2 = 0.1$ $x_1 = 0.4, x_2 = 0.8$	$x \in [0, 1.5]$ $t \in [0, 2]$
4) Linearized Burgers	$u_t + v_1 u_x - v_2 u_{xx} = 0$ $v_1 = 1, v_2 = 0.02$	$u(x, t = 0) = me^{-(kx)^2}$ $k = 2, m = 10$	$x \in [-1.5, 4.5]$ $t \in [0, 2]$
5) Non-linear Burgers	$u_t + uu_x - v_1 u_{xx} = 0$ $v_1 = 0.001$	$u(x, t = 0) = me^{-(kx)^2}$ $k = 2, m = 1$	$x \in [-2, 2]$ $t \in [0, 2]$

1. **Steady state convection-diffusion equation** is an ordinary differential equation that describes the final distribution of a scalar quantity, such as heat or mass, in one spatial dimension in the presence of both convective transport and diffusion. It is commonly used to model transport phenomena in engineering and scientific applications. Using this equation, we simulate the temperature in a spatial domain.
2. **Projectile motion equation** is an ordinary differential equation that governs the motion of an object in a horizontal plane under the influence of gravity g . The motion of the object is described by the laws of classical mechanics and can be modelled using equations of motion. Using this equation, we simulate the projectile motion of an object released with a pre-determined initial velocity and angle of attack assuming that there is no drag and a hypothetical $g \approx 3.7$ (e.g., on Mars).
3. **The Korteweg-De Vries (KdV) equation** is a partial differential equation that describes the behaviour of weakly nonlinear, dispersive waves such as those that occur in shallow water or plasmas. The KdV equation is a simple but powerful model that captures the essential physics of these wave phenomena and has been widely used in a variety of applications, including fluid mechanics, plasma physics, and nonlinear optics. Using this equation, we simulate the collision of two waves of different magnitudes traveling from different locations.
4. **The linearized Burgers' equation** is a partial differential equation that describes the behaviour of viscous, inviscid flow in one spatial dimension. It is a simplified version of the more general Burgers' equation, which is used to model the behaviour of fluid flow in the presence of shock waves and other complex phenomena. Using this

equation, we simulate the propagation of a single waveform at constant velocity.

5. **The non-linear Burgers' equation** is a partial differential equation that describes the behaviour of viscous, inviscid flow in one spatial dimension. It is a more complex and realistic model than the linear Burgers' equation and is used to study the behaviour of fluid flow in the presence of shock waves and other complex phenomena. Using this equation, we simulate the propagation of a single waveform leading to the formation of shock front.

V. PERFORMANCE METRICS

Three performance metrics were used to evaluate the effectiveness and efficiency of the optimization methods: training time, training loss, and prediction MSE.

5.1 Training Time

Training time is the amount of time it takes for the optimization method to train the PINN model. There are several factors that can affect the training time of the PINN model, including the sample size of the training data, the complexity of the physical laws being modelled, the number of network parameters, and the computational resources available for training. Detailed descriptions of these factors are provided in subsequent sections to facilitate comparison across different optimization methods.

5.2 Training Loss

Training loss is a measure of the difference between the predictions made by the PINNs and the known physical laws governing the system being modelled during training. It is calculated by summing the difference between the predicted outputs and the true values at the initial and boundary conditions, as well as the residual of the partial differential equation (PDE) representing the physical laws as shown in

Equation 1 where the weights of the loss terms, or the relative importance of each term in the loss function is kept equal at one. This difference, or violation from the governing physics, is quantified using a loss function (\mathcal{L}_{PINN}) as summarised in Table III for each benchmark problem. The training loss is used to evaluate the network's performance during the training process. The goal of each optimization method is to train the PINN models to minimize the training loss, such that the PINNs' predictions are as close as possible to the true physical system.

5.3 Prediction Mean Squared Error

The prediction mean squared error (MSE) refers to the error between the predicted solution and the ground truth

Table III: Loss formulation for benchmark problems.

Problem	Training loss
1) Convection-diffusion	$\mathcal{L}_{PINN} = \mathcal{L}_{PDE} + \mathcal{L}_{BC}$ $\mathcal{L}_{PDE} = \frac{1}{n} \sum_x (v\hat{u}_x(x) - k\hat{u}_{xx}(x))^2$ $\mathcal{L}_{BC} = \frac{1}{2} \left[(u(x=0) - \hat{u}(x=0))^2 + (u(x=1) - \hat{u}(x=1))^2 \right]$
2) Projectile motion	$\mathcal{L}_{PINN} = \mathcal{L}_{PDE_1} + \mathcal{L}_{PDE_2} + \mathcal{L}_{IC_1} + \mathcal{L}_{IC_2} + \mathcal{L}_{IC_3} + \mathcal{L}_{IC_4}$ $\mathcal{L}_{PDE_1} = \frac{1}{n} \sum_t (\hat{x}_{tt}(t))^2$ $\mathcal{L}_{PDE_2} = \frac{1}{n} \sum_t (\hat{y}_{tt}(t) + g)^2$ $\mathcal{L}_{IC_1} = (x(t=0) - \hat{x}(t=0))^2$ $\mathcal{L}_{IC_2} = (y(t=0) - \hat{y}(t=0))^2$ $\mathcal{L}_{IC_3} = (x_t(t=0) - \hat{x}_t(t=0))^2$ $\mathcal{L}_{IC_4} = (y_t(t=0) - \hat{y}_t(t=0))^2$
3) Korteweg-De Vries (KdV)	$\mathcal{L}_{PINN} = \mathcal{L}_{PDE} + \mathcal{L}_{IC}$ $\mathcal{L}_{PDE} = \frac{1}{n} \sum_{x,t} (\hat{u}_t(x,t) + v_1\hat{u}(x,t)\hat{u}_x(x,t) + v_2\hat{u}_{xxx}(x,t))^2$ $\mathcal{L}_{IC} = \frac{1}{n_{x t=0}} \sum_{x t=0} (u(x,t=0) - \hat{u}(x,t=0))^2$
4) Linearized Burgers	$\mathcal{L}_{PINN} = \mathcal{L}_{PDE} + \mathcal{L}_{IC}$ $\mathcal{L}_{PDE} = \frac{1}{n} \sum_{x,t} (\hat{u}_t(x,t) + v_1\hat{u}_x(x,t) - v_2\hat{u}_{xx}(x,t))^2$ $\mathcal{L}_{IC} = \frac{1}{n_{x t=0}} \sum_{x t=0} (u(x,t=0) - \hat{u}(x,t=0))^2$
5) Non-linear Burgers	$\mathcal{L}_{PINN} = \mathcal{L}_{PDE} + \mathcal{L}_{IC}$ $\mathcal{L}_{PDE} = \frac{1}{n} \sum_{x,t} (\hat{u}_t(x,t) + \hat{u}(x,t)\hat{u}_x(x,t) - v_1\hat{u}_{xx}(x,t))^2$ $\mathcal{L}_{IC} = \frac{1}{n_{x t=0}} \sum_{x t=0} (u(x,t=0) - \hat{u}(x,t=0))^2$

solution. It is calculated by taking the average of the squared difference between the model's predictions and the true target values. The prediction MSE is important because it provides

validation of the model's performance that is independent of the training loss.

To calculate the prediction MSE, we need to have access to the ground truth solution for each benchmark problem. For the convection-diffusion and the projectile motion problems, the ground truth solution can be found analytically. In contrast, the ground truth solution for the Korteweg-De Vries (KdV), the linearized Burgers, and the non-linear Burgers' problems are obtained by utilizing a finite volume scheme for spatial terms, while the temporal terms are integrated by second order Runge-Kutta method. To ensure convective stability, the convection terms are approximated by second order dispersion-relation preserving finite volume scheme [20], together with universal limiter [21]. The remaining spatial terms are approximated by central difference scheme.

A lower prediction MSE against the ground truth solution indicates better performance of the optimization method in training the PINN model.

VI. EXPERIMENTAL STUDY

This section presents results from using evolutionary algorithms to solve the five benchmark problems. These results indicate that evolutionary algorithms, specifically CMA-ES, can be effective at solving PINN problems, even as compared to SGD.

6.1 Configurations of PINNs and Optimization Algorithms

A preliminary investigation was conducted to explore the relationship between neural network size and model performance by varying the number of neurons in the hidden layers. An adequate neural network size was selected for each problem to ensure good approximations of the solutions to the differential equations. Additionally, we carried out a hyperparameter search to identify the best optimization settings for both CMA-ES and SGD. For CMA-ES, we tested a range of population sizes (20, 50, 80, 100) and initial standard deviations of the Gaussian distribution model (0.001, 0.005, 0.01, 0.05, 0.1, 0.5). For SGD, we tested a range of learning rates (0.001, 0.005, 0.01, 0.05, 0.1, 0.5) and minibatch sampling size of collocation points for both interior domain (10, 100, 1000) and boundary/initial points (5, 50) for benchmark problems 3-5. In prior PINN work, other authors have reported that the use of gradient-based optimizers like full-batch L-BFGS can improve the PINN model performance [1]. Hence, in the context of this work, where the neural network parameters are relatively fewer and memory scalability is not an issue, we report results from SGD optimized with both the optimal mini-batch size from hyperparameter search and without mini-batching (similar to batch gradient descent (batch GD)) for completeness. The configurations of the PINNs and best settings for both optimization algorithms used for each benchmark problem can be found in Table IV.

6.2 Baseline Results

In this study, five independent runs of each of the optimization methods were performed and the convergence trends were plotted against time up to 180s (Fig. 4). The bold lines on the plot represent the median convergence path, and the shaded areas indicate the range of values from the minimum to the maximum convergence path across the five runs. These results provide interesting insights into the

Table IV: Configurations of PINNs and optimization algorithms.

Problem	PINN architecture*	Loss evaluation: no. collocation points (incl. IC/BC points)	CMA-ES population size & initial standard deviation	SGD mini-batch size (interior + IC/BC points) & learning rate
1) Convection-diffusion	$(x) - 10 - 10 - 10 - (\hat{u})$ no. network weights = 250	10,000 (2)	80, 5e-2	100 + 2, 1e-3
2) Projectile motion	$(t) - 8 - 8 < \begin{smallmatrix} 8 - (\hat{x}) \\ 8 - (\hat{y}) \end{smallmatrix}$ no. network weights = 240	10,000 (1)	80, 1e-3	100 + 1, 1e-3
3) Korteweg-De Vries (KdV)	$\begin{smallmatrix} (x) \\ (t) \end{smallmatrix} > 8 - 8 - 8 - 8 - (\hat{u})$ no. network weights = 240	15,477 (77)	50, 5e-2	100 + 5, 1e-1
4) Linearized Burgers	$\begin{smallmatrix} (x) \\ (t) \end{smallmatrix} > 10 - 10 - 10 - (\hat{u})$ no. network weights = 260	38,793 (193)	50, 1e-2	100 + 5, 1e-2
5) Non-linear Burgers	$\begin{smallmatrix} (x) \\ (t) \end{smallmatrix} > 8 - 8 - 8 - (\hat{u})$ no. network weights = 176	25,929 (129)	100, 1e-2	100 + 5, 1e-1

*For the PINN architecture, the numbers in between input and output represent the number of nodes in hidden layers. For example, $(x) - 10 - 10 - 10 - (\hat{u})$ indicates a neural network with single input x , followed by 3 hidden layers with 10 nodes in each layer, and a single output \hat{u} . All hidden layers, except the final hidden layer, include a bias term and use *tanh* activation function. The final hidden layer uses *linear* activation function and does not include a bias term.

convergence behaviours of the optimization algorithms, which will be discussed in more detail in section 6.2.1 and 6.2.2.

6.2.1 CMA-ES JAX vs CMA-ES TensorFlow

The differences in performance between the CMA-ES implementations on JAX and TensorFlow with GPU

acceleration are particularly evident in the loss convergence plot (Fig. 4) for the convection-diffusion equation. The CMA-ES implementation on JAX is able to converge much faster than the TensorFlow implementation even with GPU acceleration. In fact, the TensorFlow implementation takes longer than 180s to converge, with the loss beginning to drop noticeably only much later (beyond the range of the plot).

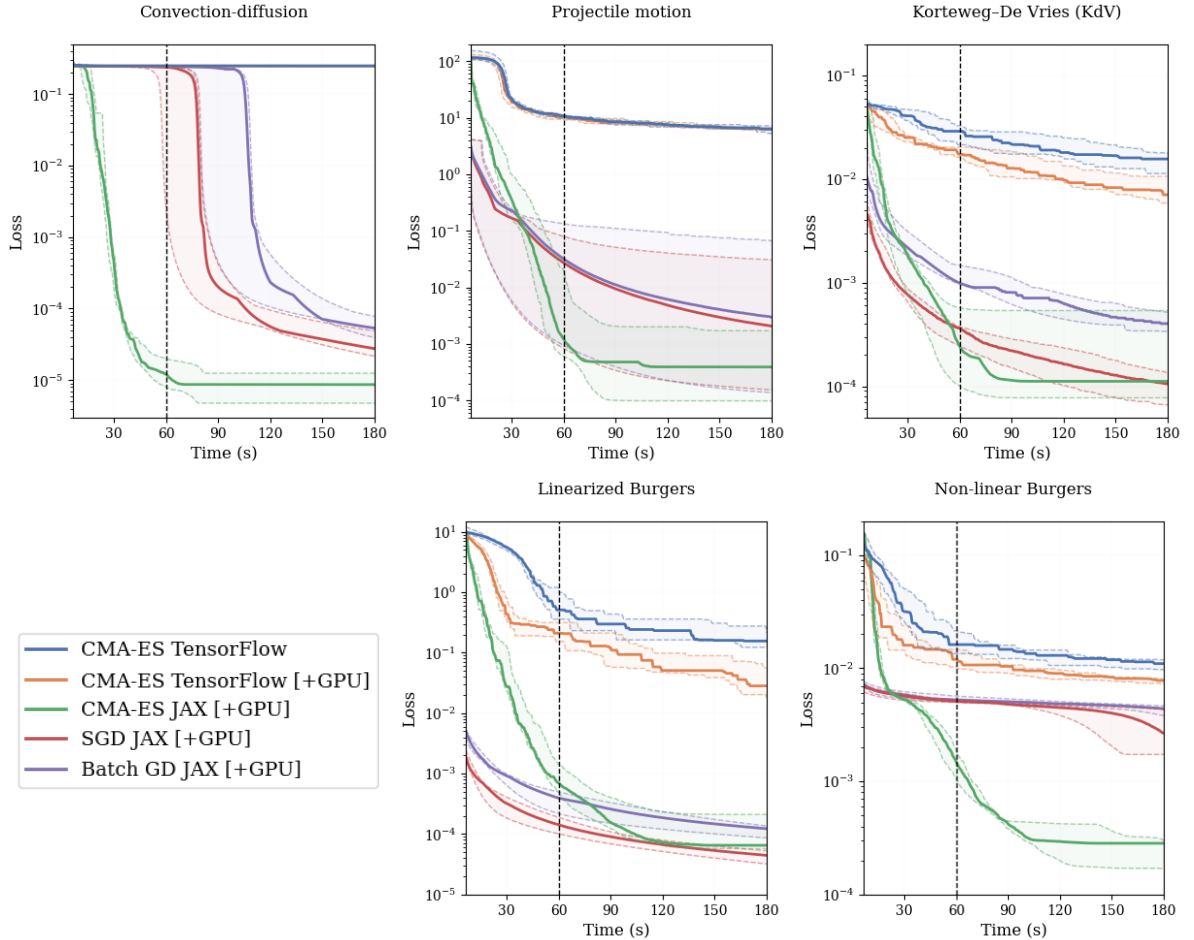


Fig. 4. Loss convergence plots.

Table V: Training loss and prediction MSE against ground truth solution at 60 seconds. In all cases, the prediction MSE is lowest for neuroevolution with CMA-ES.

Problem	Optimizer (JAX)	Training loss	Prediction MSE
1) Convection-diffusion	CMA-ES	1.00e-5	6.38e-9
	SGD	2.40e-1	1.59e-1
	Batch GD	2.44e-1	1.64e-1
2) Projectile motion	CMA-ES	6.73e-4	3.96e-4
	SGD	1.27e-1	5.50e+0
	Batch GD	1.79e-1	6.24e+0
3) Korteweg-De Vries (KdV)	CMA-ES	1.02e-4	7.57e-5
	SGD	3.12e-4	7.33e-4
	Batch GD	8.73e-4	8.53e-4
4) Linearized Burgers	CMA-ES	1.07e-3	1.27e-4
	SGD	8.50e-5	4.84e-4
	Batch GD	1.50e-4	7.13e-4
5) Non-linear Burgers	CMA-ES	1.22e-3	6.82e-4
	SGD	4.84e-3	5.92e-3
	Batch GD	5.29e-3	6.88e-3

Additionally, Fig. 4 also indicates that the use of GPU acceleration may not significantly improve the performance of the TensorFlow implementation of CMA-ES. This further highlights how the JAX framework is able to better utilize the available hardware out-of-the-box, as compared to the TensorFlow framework, which may require more customization. Since the CMA-ES implementation on JAX is able to converge much faster (in terms of wall-clock time) than the TensorFlow implementation, we conduct all subsequent baseline comparisons with their implementations on JAX. Nonetheless, it is important to note that the CMA-ES algorithms implemented on JAX and TensorFlow are from different sources and hence may bear some variation in the implementation of the original algorithm.

6.2.2 CMA-ES JAX vs SGD JAX

Fig. 4 shows that CMA-ES, when run on JAX, typically converges to the minimum much faster than SGD run on JAX. The plots of loss convergence for both optimizers show that the trends intersect, indicating that the two optimizers perform differently at different stages of the convergence process, hence pointing to possible future hybridizations that leverage the best of both worlds. The results also suggest that SGD typically converges more slowly than CMA-ES. This difference in performance may be due to the fact that CMA-ES is better at solving complex PINN optimization landscapes with many local optima, as it uses multiple samples (whose spread is determined by the covariance matrix of the underlying Gaussian distribution model) to explore the search space. It can therefore more effectively navigate across a complex landscape with local optima, whereas gradient

descent is faced with a more difficult task of finding a continuous path of least resistance across the landscape [7]. In addition, SGD is less effective as it can become biased towards local optima if they exist near its initialization, delaying the onset of convergence (e.g., in the convection-diffusion problem).

In a practical context, it is important that PINN training be completed in a reasonable amount of time. Hence, we further compare the training loss and prediction MSE attained by both optimizers after 60 seconds of training. The best MSE predictions are highlighted in bold in Table V.

The results show that CMA-ES outperforms SGD on training loss for four out of the five benchmark problems. *Importantly, CMA-ES generates the lowest prediction MSE against the ground truth for all five benchmark problems.* To visualize the results, we plotted the solutions generated by CMA-ES JAX and SGD JAX after 60 seconds of training (Fig. 5-9). In the linearized Burgers' (Fig. 8) problem, the solution generated by both optimizers are visually similar to the simulated solutions. However, for the convection-diffusion (Fig. 5), projectile motion (Fig. 6), KdV (Fig. 7), and non-linear Burgers' (Fig. 9) problems, the solution generated by CMA-ES is noticeably more similar to the ground truth than the solution generated by SGD. The absolute error plots in Fig. 7, 8 and 9 clearly illustrate the accuracy of the predicted solution, with a smaller error for solutions generated by CMA-ES indicating a better match to the true target solutions.

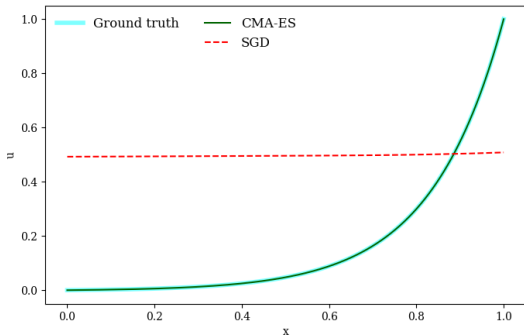


Fig. 5. PINN solution for convection-diffusion problem after 60 seconds of training.

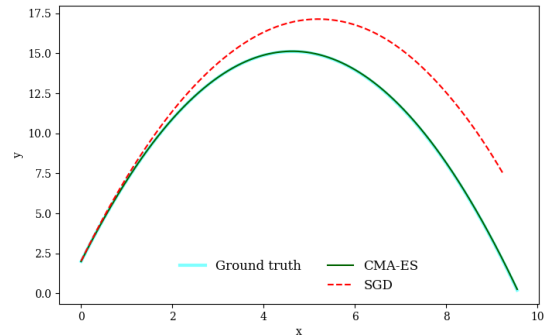


Fig. 6. PINN solution for projectile motion problem after 60 seconds of training.

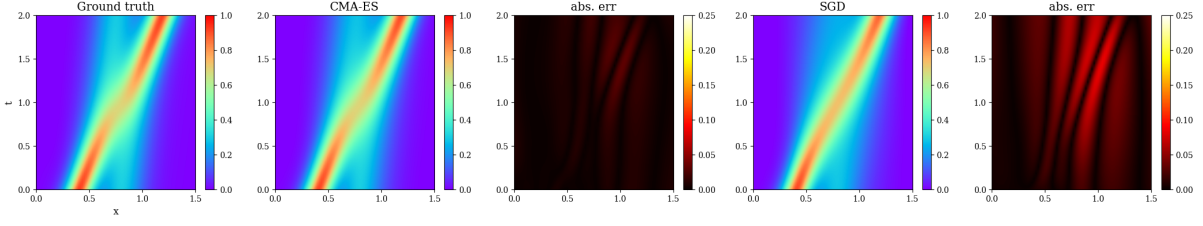


Fig. 7. PINN solution for Korteweg–De Vries (KdV) problem *after 60 seconds of training*.

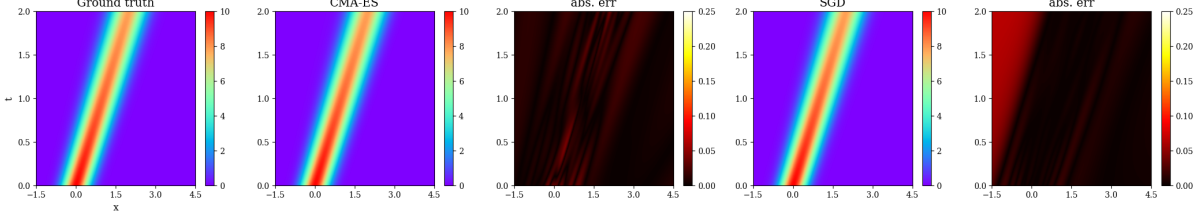


Fig. 8. PINN solution for linearized Burgers' problem *after 60 seconds of training*.

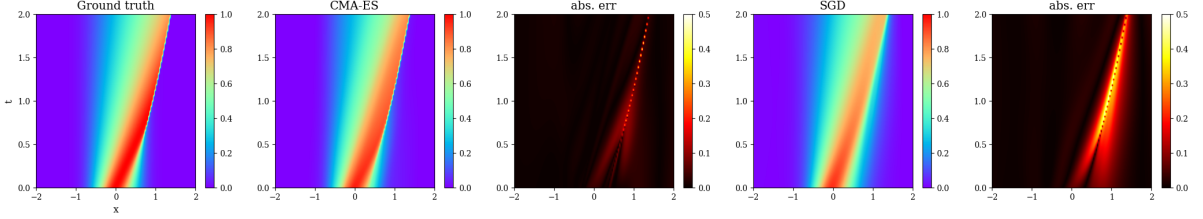


Fig. 9. PINN solution for non-linear Burgers' problem *after 60 seconds of training*.

VII. CONCLUSION

We examined the reasons behind the effectiveness of SGD variants in optimizing Deep Neural Networks (DNNs) and its implications for choice of optimizers for PINNs. Our analysis revealed that the presence of spurious local minima in proximity to the initialization point may pose challenges to the effectiveness of conventional optimizer choices like SGD. In light of these findings, we established the necessity to explore alternative optimization techniques, such as neuroevolution, which exhibit a greater capability for exploring the loss landscape and avoiding deceptive local minima. We designed five PINN benchmark problems and evaluated the performance of different optimization methods and implementation backends on these benchmark problems. We demonstrated that evolutionary algorithms, as exemplified by CMA-ES, have the potential to be more effective at solving these problems than SGD. Importantly, CMA-ES generates the lowest prediction MSE against the ground truth for all five benchmark problems after 60 seconds of training. While these results do not prove that EAs will surpass SGD for all PINN problems, they are an intriguing hint that the potential for EAs in this area may be greater than previously believed. At the least it suggests that the exploration and development of alternative optimization algorithms, including evolutionary algorithms, for the complex task of optimizing PINNs is warranted so as to tackle other complex, real-world engineering problems and challenges. We provided the link <https://github.com/nicholassung97/Neuroevolution-of-PINNs> on Github for the JAX and TensorFlow implementations of all benchmark problems, and analytical and simulation solutions as supplementary material.

REFERENCES

- [1] M. Raissi, P. Perdikaris, and G.E. Karniadakis, "Physics-informed neural networks: A deep learning framework for solving forward and inverse problems involving nonlinear partial differential equations," *J. Comput. Phys.*, vol. 378, pp. 686–707, 2019.
- [2] G.E. Karniadakis, I.G. Kevrekidis, L. Lu, P. Perdikaris, S. Wang, and L. Yang, "Physics-informed machine learning," *Nature Reviews Physics*, vol. 3, no. 6, pp. 422–440, 2021.
- [3] A.S. Krishnapriyan, A. Gholami, S. Zhe, R.M. Kirby, and M.W. Mahoney, "Characterizing possible failure modes in physics-informed neural networks," in *Proc. Adv. Neural Inf. Process. Syst.*, vol. 32, pp. 26548–26560, 2021.
- [4] T. de Wolff, H.C. Lincopi, L. Martí, and N. Sanchez-Pi, "MOPINNs: An Evolutionary Multi-Objective Approach to Physics-Informed Neural Networks," in *Proc. 2022 Genetic and Evolutionary Computation Conference Companion, GECCO '22*, pp. 228–231, 2022.
- [5] N. Rahaman, A. Baratin, D. Arpit, F. Draxler, M. Lin, F.A. Hamprecht, Y. Bengio, and A. Courville, "On the Spectral Bias of Neural Networks," in *Proc. 36th Int'l Conf. on Machine Learning, ICML 2019*, vol. 2019-June, pp. 9230–9239, 2019.
- [6] J.C. Wong, C. Ooi, A. Gupta, and Y.-S. Ong, "Learning in Sinusoidal Spaces with Physics-Informed Neural Networks," *IEEE Trans. on Artificial Intelligence*, vol. 0, no. 0, pp. 1–15, 2022.
- [7] T. Garipov, P. Izmailov, D. Podoprikin, D. Vetrov, and A.G. Wilson, "Loss Surfaces, Mode Connectivity, and Fast Ensembling of DNNs," in *Proc. Adv. Neural Inf. Process. Syst.*, vol. 2018-December, pp. 8789–8798, 2018.
- [8] F.M. Rohrhofer, S. Posch, and B.C. Geiger, "On the Pareto Front of Physics-Informed Neural Networks," [Online]. Available: <https://arxiv.org/abs/2105.05328>, 2021.
- [9] V. Gopakumar, S. Pamela, and D. Samaddar, "Loss Landscape Engineering via Data Regulation on PINNs," [Online]. Available: <https://arxiv.org/abs/2102.00058>, 2022.
- [10] G. Morse and K. O. Stanley, "Simple evolutionary optimization can rival stochastic gradient descent in neural networks," in *Proceedings of the 2016 Genetic and Evolutionary Computation Conference (GECCO 2016)*, pp. 477–484, 2016.

- [11] K. O. Stanley, J. Clune, J. Lehman, and R. Miikkulainen, "Designing neural networks through neuroevolution," *Nature Machine Intelligence*, vol. 1, no. 1, pp. 24-35, 2019.
- [12] J. C. Wong, A. Gupta, and Y.-S. Ong, "Can Transfer Neuroevolution Tractably Solve Your Differential Equations?," *IEEE Computational Intelligence Magazine*, vol. 16, pp. 14-30, 2021.
- [13] N. Hansen, "The CMA Evolution Strategy: A Comparing Review," in *Towards a New Evolutionary Computation*, pp. 75-102, 2006.
- [14] Y. Tang, Y. Tian, and D. Ha, "EvoJAX: Hardware-Accelerated Neuroevolution," in *Proceedings of the 2022 Genetic and Evolutionary Computation Conference (GECCO 2022 Companion)*, pp. 308-311, 2022.
- [15] M. Abadi, et al., "TensorFlow: Large-Scale Machine Learning on Heterogeneous Distributed Systems," 2016.
- [16] L. A. Prendergast and J. A. Smith, "Sensitivity of principal hessian direction analysis," *Electronic Journal of Statistics*, vol. 1, pp. 253-267, 2007.
- [17] N. Hansen, "The CMA Evolution Strategy: A Tutorial," 2016.
- [18] J. Bradbury, R. Frostig, P. Hawkins, M.J. Johnson, C. Leary, D. Maclaurin, G. Necula, A. Paszke, J. VanderPlas, S. Wanderman-Milne, Q. Zhang, "JAX: composable transformations of Python+NumPy programs," 2018.
- [19] J. Van den Bossche, "Need for Speed: JAX. Training your neural network ten times....," *ML6team*, (n.d.).
- [20] P. H. Chiu, "An improved divergence-free-condition compensated method for solving incompressible flows on collocated grids," *Computers & Fluids*, vol. 162, pp. 39-54, 2018.
- [21] B.P. Leonard, "The ULTIMATE conservative difference scheme applied to unsteady one-dimensional advection," *Comput Methods Appl Mech Eng.*, vol. 88, pp. 17-74, 1991.